Enhanced $\chi^{(3)}$ interactions of unamplified femtosecond Cr:forsterite laser pulses in photonic-crystal fibers

Aleksandr N. Naumov, Andrei B. Fedotov, and Aleksei M. Zheltikov

Physics Department, International Laser Center, M.V. Lomonosov Moscow State University, 119899 Moscow, Russia

Vladislav V. Yakovlev

Department of Physics, University of Wisconsin—Milwaukee, 1900 East Kenwood Boulevard, 53211 Milwaukee, Wisconsin

Leonid A. Mel'nikov

Saratov State University, Astrakhanskaya ulitsa 83, 410026 Saratov, Russia

Valentin I. Beloglazov, Nina B. Skibina, and Andrei V. Shcherbakov

Technology and Equipment for Glass Structures Institute, prospekt Stroitelei, 410044 Saratov, Russia

Received November 28, 2001; revised manuscript received April 8, 2002

Enhancement of nonlinear optical interactions in the core of a photonic-crystal fiber allows several $\chi^{(3)}$ processes to be simultaneously observed in the field of unamplified 30-fs pulses of a Cr:forsterite laser. Subnanojoule fundamental-radiation pulses of this laser experience spectral broadening arising from self-phase modulation and generate the third harmonic at 410–420 nm. Third-harmonic pulses also appear spectrally broadened at the output of the fiber as a result of the cross-phase-modulation effect. This catalog of enhanced $\chi^{(3)}$ processes observed in photonic-crystal fibers opens the way for using such fibers for frequency conversion of low-energy femtosecond pulses with simultaneous chirp control and subsequent pulse compression.

OCIS codes: 190.4370, 190.4380, 320.7140.

1. INTRODUCTION

Microstructure (or holey) fibers,[1–7] i.e., fibers in which a cladding has the form of a two-dimensional (often periodic, i.e., photonic-crystal) array of closely packed glass capillaries drawn at a high temperature, were recently shown to considerably enhance various nonlinear optical processes as a result of the high degree of light localization in the fiber core.[8–13] High light intensities, attainable by coupling nonamplified femtosecond laser pulses into the small core of a holey fiber, allowed the observation of enhanced spectral broadening of ultrashort laser pulses,[11] self-phase modulation (SPM),[13] and supercontinuum generation[10] starting with subnanojoule energies of Ti:sapphire laser pulses. Second- and third-harmonic generation (THG) in holey fibers was also demonstrated by Ranka *et al.*[12] using a *Q*-switched Nd:YAG laser operating at 1064 nm. Some of these nonlinear optical processes have already found extensive applications in various areas of modern optics. In particular, femtosecond frequency combs broadened to span more than an octave in holey[14–17] (as well as tapered[18,19]) fibers are now used as frequency rulers, leading to revolutionary changes in optical frequency metrology.[14–17,20]

Many applications of short laser pulses with broad spectra in pulse compression and coherent optics (including coherent spectroscopy and optical coherence tomography,[21,22] for example) require a controlled distribution of the laser field phase within the spectrum of the pulse. This phase controllability of the broad spectra of laser pulses is usually difficult to attain in the regime of supercontinuum generation. In addition, serving as a convenient broadband source for various spectroscopic applications, supercontinua produced in microstructure fibers become much less useful whenever a high spectral density of laser energy is necessary within a certain spectral range. Nonlinear optical techniques based on harmonic generation and wave mixing seem to be more adequate in such situations.

In this paper we demonstrate that the high degree of light localization in the core of a photonic-crystal fiber (PCF) enhances third-order nonlinear optical processes, allowing the third harmonic of nonamplified Cr:forsterite laser pulses to be generated and simultaneously offering the possibility of controlling the chirp of the third-harmonic pulse through the cross-phase modulation (XPM) effect. This observation of a XPM-chirp-controlled THG process adds XPM to the catalog of nonlinear optical processes observed in microstructure fibers, thus opening

0740-3224/2002/092183-08$15.00

the way for using these fibers for frequency conversion with simultaneous chirp control or pulse compression.

2. BASIC RELATIONS FOR CROSS-PHASE-MODULATION-CHIRP-CONTROLLED THIRD-HARMONIC GENERATION

A. Amplitude and Phase of the Third-Harmonic Pulse

The third-harmonic pulse generated in the field of a short pump pulse in a fiber may acquire a pump-intensity-dependent phase shift that is due to XPM.[23] Thus, by varying the amplitude of the fundamental pulse, as shown in earlier work,[24,25] one can control the spectrum of the third harmonic emerging from a fiber and optimize conditions for subsequent pulse compression. Physically, the possibility of implementing such an XPM control of the chirp of optical harmonics is associated with the fact that the third harmonic is produced in the field of a self-phase-modulated fundamental pulse while the phase of the third harmonic is modulated by the change in the refractive index induced by the fundamental pulse.

We consider in the theoretical part of this paper a generic model of THG by a pump pulse with the central frequency ω in a fiber without explicitly specifying the field distribution and dispersion of waveguide modes. We assume that the THG process involves a pair of waveguide modes with a minimum phase mismatch, and we formally introduce propagation constants and field distributions of pump and third-harmonic radiation corresponding to these waveguide modes. Then, in accordance with the results of the slowly varying envelope analysis of THG in a fiber with a first-order dispersion,[24,25] the amplitudes of the pump and the third-harmonic pulses, $A(\eta_p, z)$ and $B(\eta_h, z)$, can be represented as

$$A(\eta_p, z) = A_0(\eta_p)\exp[i\varphi_{\mathrm{SPM}}(\eta_p, z)], \tag{1}$$

$$\begin{aligned} B(\eta_h, z) = {} & i\beta\exp[i\varphi_{\mathrm{XPM}}(\eta_h, z)] \\ & \times \int_0^z \mathrm{d}z' A_0^3(\eta_h + \varsigma z')\exp[-i\Delta k z' \\ & + 3i\varphi_{\mathrm{SPM}}(\eta_h + \zeta z', z') \\ & - i\varphi_{\mathrm{XPM}}(\eta_h, z')], \end{aligned} \tag{2}$$

where $\eta_l = (t - z/v_l)/\tau$ is the time in the frame of reference running along the propagation coordinate z with the pump or the third-harmonic pulse ($l = p, h$, with subscripts p and h corresponding to the parameters of the pump and third-harmonic pulses, respectively) normalized to the duration τ of the incident pump pulse; v_p and v_h are the group velocities of the pump and the third-harmonic pulses, respectively; $\varsigma = (1/v_h - 1/v_p)/\tau$; $\Delta k = K_h - 3K_p$ is the phase mismatch; K_p and K_h are the propagation constants of the pump and the third-harmonic pulses corresponding to the relevant eigenmodes of the fiber; $A_0(\eta_p)$ is the envelope of the pump pulse at the input of the fiber;

$$\varphi_{\mathrm{SPM}}(\eta_p, z) = \gamma_1|A_0(\eta_p)|^2 z \tag{3}$$

is the nonlinear phase of the pump pulse that is due to SPM; and

$$\varphi_{\mathrm{XPM}}(\eta_h, z) = 2\gamma_2\int_0^z |A_0(\eta_h + \varsigma z')|^2\mathrm{d}z' \tag{4}$$

is the nonlinear phase of the third-harmonic pulse that is due to modulation of the refractive index induced in the medium by the pump pulse at the frequency of the third harmonic. The nonlinear coefficients γ_1, γ_2, and β, appearing in Eqs. (2)–(4) can be expressed in terms of the nonlinear optical cubic susceptibilities $\chi^{(3)}(\omega_q;\omega_1, \omega_2, \omega_3)$ with the relevant frequency arguments ($\omega_q = \omega_1 + \omega_2 + \omega_3$) responsible for SPM, XPM, and THG, respectively[25]:

$$\gamma_1 = \frac{3\pi\omega^2}{2K_p c^2}\chi^{(3)}(\omega;\omega, -\omega, \omega)\frac{\iint [f_p(\rho)]^4\rho\mathrm{d}\rho\mathrm{d}\theta}{\iint [f_p(\rho)]^2\rho\mathrm{d}\rho\mathrm{d}\theta}, \tag{5}$$

$$\gamma_2 = \frac{27\pi\omega^2}{2K_h c^2}\chi^{(3)}(3\omega;3\omega, -\omega, \omega) \times \frac{\iint [f_h(\rho)]^2[f_p(\rho)]^2\rho\mathrm{d}\rho\mathrm{d}\theta}{\iint [f_h(\rho)]^2\rho\mathrm{d}\rho\mathrm{d}\theta}, \tag{6}$$

$$\beta = \frac{9\pi\omega^2}{2K_h c^2}\chi^{(3)}(3\omega;\omega, \omega, \omega) \times \frac{\iint f_h(\rho)[f_p(\rho)]^3\rho\mathrm{d}\rho\mathrm{d}\theta}{\iint [f_h(\rho)]^2\rho\mathrm{d}\rho\mathrm{d}\theta}, \tag{7}$$

where $f_p(\rho)$ and $f_h(\rho)$ are the transverse distributions of the field in the pump beam and the third harmonic corresponding to the relevant eigenmodes of the fiber and ρ and θ are the modulus of the radius vector and the azimuthal angle in the cross section of the fiber. Since we restrict ourselves to the first-order approximation of dispersion theory, the pump pulse in our model propagates through the fiber with no changes in its envelope, $|A(\eta_p, z)| = |A_0(\eta_p)|$.

We consider pump pulses with a hyperbolic secant envelope:

$$A_0(\eta_p) = \tilde{A}\frac{\exp[i\varphi_0(\eta_p)]}{\cosh\eta_p}, \tag{8}$$

where $\varphi_0(\eta_p) = \arg[A_0(\eta_p)]$ is the initial chirp of the pump pulse. The nonlinear phase $\varphi_{\mathrm{XPM}}(\eta_h, z)$ given by Eq. (4) can then be calculated analytically:

$$\varphi_{\mathrm{XPM}}(\eta_h, z) = \frac{2\gamma_2\tilde{A}^2}{\zeta}[\tanh(\eta_h + \zeta z) - \tanh(\eta_h)]. \tag{9}$$

Introducing a new integration variable $x = \eta_h + \zeta z'$, we can reduce Eq. (2) to the following form:

$$B(\eta_h, z) = i\frac{\beta\tilde{A}^3}{\varsigma}\exp\left[i\frac{2\gamma\tilde{A}^2}{\varsigma}\tanh(\eta_h + \varsigma z) - i\frac{\Delta k}{\varsigma}\eta_h\right] \times \int_{\eta_h}^{\eta_h+\varsigma z} dx \frac{1}{\cosh(x)^3}\exp\left[-i\frac{\Delta k}{\zeta}x + i3\varphi_0(x) + i\frac{3\gamma_1\tilde{A}^2(x-\eta_h)}{\varsigma\cosh(x)^2} - i\frac{2\gamma_2\tilde{A}^2}{\varsigma}\tanh(x)\right]. \quad (10)$$

Formulas (9) and (10) allow the XPM-induced phase shift and the amplitude of the third-harmonic pulse to be calculated very conveniently, providing a clear physical understanding of the main features observed in the spectra of the third harmonic generated under these conditions. In particular, Eq. (10) shows that the third harmonic is generated mainly around the maximum of the pump pulse, i.e., within the area where $|x| \leqslant 1$ (i.e., $|t - z'/v_p| \leqslant \tau$). It should be noted that, since the analysis performed in this section was based on the slowly varying envelope approximation and effects related to the second- and higher-order dispersion effects were neglected, the results of this analysis should be used very carefully in the case of very short light pulses. Our experiments on THG in PCFs were carried out with 30-fs pulses of pump radiation. Although these pulses are still much longer than the field cycle, which allows second-order derivatives to be neglected in the relevant wave equation, second-order dispersion effects, of course, play an important role, leading to pulse spreading (see the estimates in Subsection 2.C). It is difficult to believe that the expressions derived above can provide a good approximation for the evolution of pulse envelopes under these conditions. In view of this circumstance, we focus our further consideration on the analysis of phase-matching effects instead of studying the evolution of pulse envelopes. Although perhaps not very accurate, such an approach will give us a simple quantitative (and often intuitive) understanding of changes observed in the spectrum of the third harmonic. Based on this approach, we show, in particular, that, because of the joint action of phase-mismatch and group-delay effects, phase matching in THG may be achieved for the spectral components of the pump pulse that are blueshifted relative to the central frequency of the pump pulse, which leads to the asymmetry in the spectrum of the third harmonic generated in a PCF. A similar effect was experimentally demonstrated earlier for the second harmonic generated by short laser pulses in a nonlinear crystal,[26] suggesting a convenient method for the measurement of nonlinearities in various nonlinear optical materials.

B. Phase Mismatch

Now we proceed with the analysis of phase matching for THG under conditions when SPM and XPM effects have to be taken into consideration. As follows from Eq. (2), the phase shift between the third-harmonic field and the nonlinear polarization induced in the medium at the frequency of the third harmonic can be written as

$$\Delta\varphi(\eta_h, z) = \Delta k z - 3\varphi_{\mathrm{SPM}}(\eta_h + \zeta z, z) - 3\varphi_0(\eta_h + \zeta z) + \varphi_{\mathrm{XPM}}(\eta_h, z). \quad (11)$$

Expression (11) shows that the total phase shift between the third-harmonic field and the nonlinear polarization induced in the medium at the frequency of the third harmonic is determined by the linear wave-vector mismatch related to the material dispersion, the initial phase of the pump pulse, and intensity-dependent phase shifts induced by SPM and XPM. Generalized phase matching for THG under conditions when SPM and XPM effects have to be taken into consideration can be formulated in terms of the effective wave-vector mismatch:

$$\Delta k_{\mathrm{eff}}(\eta_h, z) = \frac{\partial}{\partial z}[\Delta\varphi(\eta_h, z)]. \quad (12)$$

Perfect phase matching is achieved when this wave-vector mismatch is exactly equal to zero. When the pump field is weak, leading to negligible SPM and XPM effects, and the group delay is small, the effective wave-vector mismatch defined by Eq. (12) is reduced to

$$\Delta k_{\mathrm{eff}} = \Delta k + 3\varsigma\bar{\omega}_p(\eta_h + \zeta z, z), \quad (13)$$

where

$$\bar{\omega}_p(\eta, z) = -\frac{\partial}{\partial\eta}\arg[A(\eta, z)]$$

is the dimensionless quantity representing the deviation of the instantaneous frequency of the pump pulse from its central frequency ω in units of $1/\tau$.

According to the definitions of the parameter ζ and the group velocity, we can then represent the phase-matching condition $\Delta k_{\mathrm{eff}} = 0$ as

$$K_h + \frac{dK_h}{d\omega}\frac{3\bar{\omega}_p}{\tau} = 3\left(K_p + \frac{dK_h}{d\omega}\frac{\bar{\omega}_p}{\tau}\right). \quad (14)$$

Equation (14) shows that the joint action of phase-mismatch and group-delay effects leads to phase matching in THG for the spectral component of the pump pulse shifted by $\bar{\omega}_p/\tau$ with respect to the central frequency.

With more intense pump pulses, SPM and XPM effects lead to the spectral broadening of the pump (Fig. 1) and third-harmonic pulses, contributing to the dependence of the phase shift [Eq. (11)] and the effective wave-vector

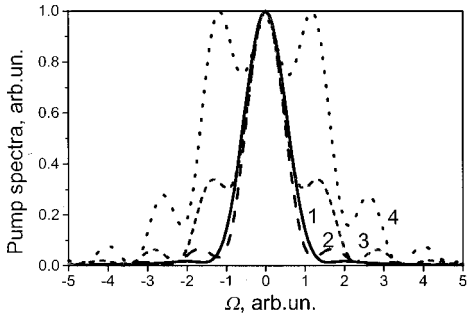

Fig. 1. Normalized spectra of a 30-fs pump pulse (8) with $\varphi_0(\eta_p) = \alpha\eta_p^4$ and $\alpha = 0.13$ (curve 1) at the input of the fiber and (curves 2–4) at the output of an 8-cm fiber with $n_2 = 3.2 \times 10^{-16}$ cm^2/W calculated with the use of Eqs. (1) and (3) for pulse energies of (curve 2) 0.1, (curve 3) 0.2, and (curve 4) 0.3 nJ.

mismatch [Eq. (12)] on the propagation coordinate and the running time η_h. This also leads, as shown in earlier work,[27] to the asymmetry of the spectral broadening of the third-harmonic pulse. In a nonlinear medium with self-focusing ($n_2 > 0$), the carrier frequency of the pump pulse is redshifted on the leading edge and blueshifted on the trailing edge of the pulse. Therefore the wave-vector mismatch on the trailing edge of the pump pulse in this case is always less than Δk_{eff} on the leading edge of this pulse, which gives rise to a predominantly blueshift of the third-harmonic spectrum. It should be noted that the asymmetry of spectral broadening of a probe pulse is generally typical of XPM when the group delay of pump and probe pulses is nonnegligible.[23] The dependence of the effective wave-vector mismatch on the internal time within the pulse adds more aspects to this asymmetric spectral broadening when the third harmonic generated in the field of a short pump pulse plays the role of the probe pulse.

Thus, as predicted by Eqs. (11)–(14), the asymmetry in the spectral broadening of the third harmonic is due to the phase matching achieved for spectral components of the broadband pump pulse blueshifted with respect to the central frequency of the pump pulse. This is exactly what we observed in our experiments on THG in a PCF, and we resort to Eqs. (11)–(14) in Section 4 of this paper to explain the asymmetry arising in the spectra of the third harmonic generated in a PCF. In Subsection 2.C we discuss in greater detail a specific regime of THG phase matching in an optical fiber, with the fundamental mode of pump radiation generating the third harmonic in Čerenkov-type fiber modes.

C. Dispersion of Photonic-Crystal Fibers and Čerenkov-Type Phase Matching of Third-Harmonic Generation in an Optical Fiber

Analysis of the dispersion of a PCF is crucial for understanding the regimes of nonlinear optical interactions in guided modes of a fiber and for optimizing parameters of the fiber for nonlinear optical frequency conversion and pulse control. In particular, the efficiency of the THG process considered in this paper is highly sensitive to fiber dispersion, which gives rise to the phase mismatch and temporal walk-off of the pump pulse and the third harmonic, also leading to group-delay and pulse-spreading effects. The possibility of tailoring the dispersion of PCFs by changing their structure is, therefore, another important and useful property of these fibers, which offers much promise for the enhancement of nonlinear optical interactions.

To assess dispersion properties of the PCFs used in our experiments, we employed standard expressions for the dispersion of a step-index fiber, replacing the refractive index of the solid fiber cladding, appearing in the standard theory of optical fibers,[23,28] with the effective refractive index introduced, after Birks *et al.*,[2] as $n_{\text{eff}} = \beta_{\text{cl}}/k$, where β_{cl} is the propagation constant of the fundamental space-filling mode, i.e., the fundamental mode of an infinite structure obtained by periodically translating a unit cell of the PCF cladding. Following the method of analysis proposed by Birks *et al.*,[2] we found an estimate of β_{cl} by solving the scalar wave equation[28] for the field distribution ψ in a circular unit cell with symmetric boundary conditions $\partial\psi/\partial s = 0$, where s is the coordinate along the axis oriented in the direction perpendicular to the boundary of the unit cell. This field distribution can be expressed in terms of zeroth-order Bessel functions. The above specified boundary condition supplemented with the continuity conditions for ψ and $\partial\psi/\partial s$ on the glass–air interface gives the characteristic equation for β_{cl}.

Solid curve 1 in Fig. 2 shows the refractive index for the bulk material of our fiber as a function of the wavelength. Our fibers were made of S93-1 glass (55% SiO_2, 30% PbO, 2.0% Al_2O_3, 3.8% Na_2O, and 9.2% K_2O) with additions of S95-2 glass (69.6% SiO_2, 4.0% Al_2O_3, 2.8% B_2O_3, 6.9% CaO, 9.0% Na_2O, and 7.7% K_2O). The optical properties of this glass were close to those of F4 flint glass.[29] In view of the composition of the material of our fibers, a standard estimate of $n_2 = 3.2 \times 10^{-16}$ cm^2/W was used for the nonlinear refractive index, which agreed well with the results of our experiments on the SPM of short laser pulses in these fibers (see Section 4).

In the limit of a weakly guiding fiber (which seems to be a reasonable approximation given the structure of the fiber used in our experiments, see Section 3), our PCF with a fiber core radius equal to 1.5 μm and the effective refractive index of the cladding estimated from β_{cl} supports a fundamental mode and the LP_{11} mode, which is a linearly polarized combination of the HE_{21}, TE_{01}, and TM_{01} waveguide modes degenerate in propagation constant. Dashed and dotted curves 2 and 3 in Fig. 2 show the wavelength dependences of the effective refractive indices for the fundamental and LP_{11} modes in a PCF with the above specified parameters. As can be seen from these dependences, as well as from Fig. 3, which shows the refractive index n, the group index n_g, and dispersion D of the bulk material of the fiber as functions of the wavelength, dispersion gives rise to a considerable phase mismatch between the pump pulse and the third harmonic ($\Delta k = 10^4$ cm^{-1} for the all-fundamental-mode THG process, corresponding to the coherence length $L_{\text{coh}} = 1/\Delta k = 1$ μm), which prevents one from achieving high THG efficiencies in the fiber modes considered. The walk-off length for 30-fs pump and third-harmonic pulses is also very short, $\approx$0.01 cm. Keeping in mind that 30-fs pulses of the third harmonic spread out to a pulse duration of the order of 100 fs (as the dispersion lengths for

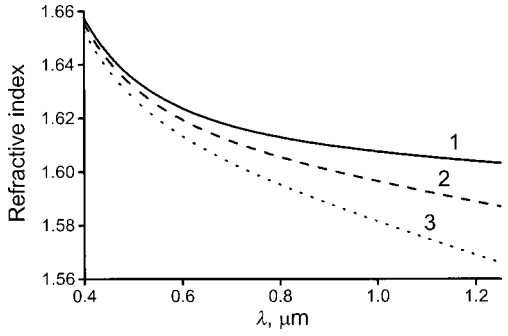

Fig. 2. Refractive index as a function of the wavelength for the bulk material of the fiber (curve 1) and the effective refractive indices calculated for (curve 2) the fundamental (curve 3) and LP_{11} modes of a PCF with an air-filling fraction of 16% and core radius of 1.5 μm. The pitch of the cladding is equal to the core radius.

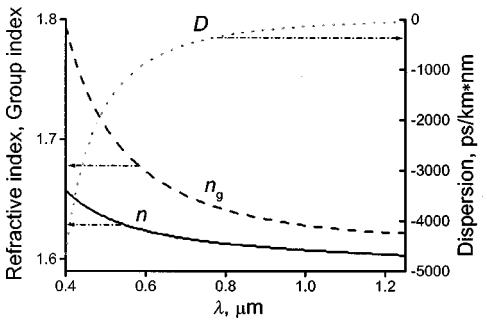

Fig. 3. Refractive index n, group index n_g, and dispersion D of the bulk material of the fiber as functions of the wavelength.

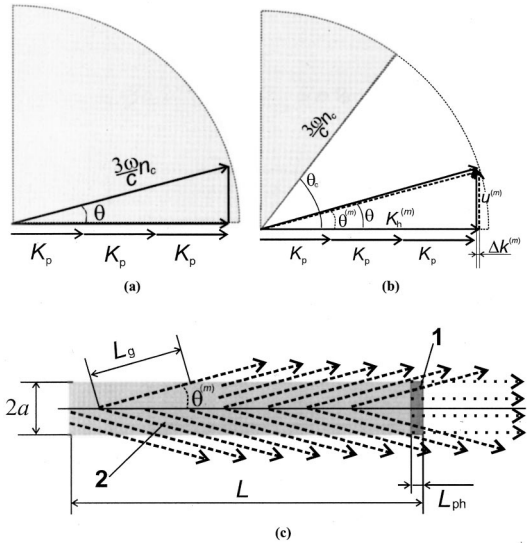

Fig. 4. Diagram of Čerenkov-type phase matching in THG in a fiber with (a) an infinite and (b) finite cladding. The angle θ corresponds to phase-matched THG. The shaded area corresponds to the range of angles where Čerenkov-type modes of the third harmonic have a continuous spectrum of propagation constants and the third harmonic may be emitted in an arbitrary direction. In the nonshaded area, Čerenkov-type modes have a discrete spectrum of propagation constants and the third harmonic may be emitted at an angle $\theta^{(m)}$ with respect to the fiber axis, with $K_h^{(m)}$ and $U^{(m)}$ being the relevant propagation constant and the transverse wave number in the fiber core. (c) Geometry of Čerenkov-phase-matched THG in a fiber. The dashed arrows show the third harmonic Čerenkov radiation emitted along the entire length L of the fiber, 2; L_g is the interaction length, bounded by the finite radius a of the pump mode. The dotted arrows show the fundamental mode of the third harmonic generated in a very thin layer, 1, with the thickness equal to the coherence length L_{ph} close to the output end of the fiber.

30-fs third-harmonic pulses in the above specified fiber modes are 0.3–0.4 cm), the walk-off length in reality is much longer, but is still not enough, of course, to allow noticeable THG.

The influence of phase-mismatch and group-delay effects may be substantially reduced, however, when the fundamental mode of pump radiation generates the third harmonic in Čerenkov-type modes[30–36] (Fig. 4). The phase mismatch in our case arises because the phase velocity of the nonlinear polarization induced in the fiber by the pump pulse at the frequency of the third harmonic is higher than the phase velocity of the electromagnetic field at the same frequency. This allows Čerenkov-type phase matching to be achieved for the THG process [Figs. 4(a) and 4(b)] at the angle θ, determined from[36]

$$\cos\theta = \tilde{n}_p/n_c, \tag{15}$$

where $\tilde{n}_p = K_p c/\omega$ is the effective refractive index for the waveguide mode of pump radiation and n_c is the refractive index of the fiber core at the frequency of the third harmonic. Since the PCF has a finite cladding in our case, the modes supported by the core + cladding fiber have a discrete spectrum, giving rise to a discrete set of angles $\theta^{(m)}$ corresponding to guided modes of the third harmonic with propagation constants $K_h^{(m)}$ and the mode parameter $U^{(m)}$ in the cladding [Fig. 4(b)]. Outside the cone bounded by the angle of total internal reflection θ_c [within the shaded area in Fig. 4(b)], the third harmonic may be emitted in any direction. Extensive earlier work[30–35] on Čerenkov-type SHG has demonstrated that Čerenkov phase matching allows high efficiencies of frequency doubling to be achieved in different types of waveguide, including periodically poled waveguides[34] with quasi-phase-matched SHG as well as planar photonic-bandgap waveguides.[35]

The length of coherent nonlinear optical interaction for the Čerenkov-type phase matching is limited by the transverse size (effective radius) of the waveguide pump mode a:

$$L_g = a/\cos\theta. \tag{16}$$

Setting n_c equal to the effective refractive index corresponding to the fundamental pump mode in the PCF considered, we arrive at the estimates $\theta = 16°$ and $L_g = 8\ \mu$m. From the analysis of the geometry of the area of nonlinear optical interaction [Fig. 4(c)], we find that the enhancement of Čerenkov-type generation of the third harmonic at the angle $\theta^{(m)}$ with respect to the fiber axis relative to THG in localized waveguide modes can be estimated as

$$C = \frac{2L}{a\sin[\theta^{(m)}]}\left(\frac{L_g}{L_{ph}}\right)^2. \tag{17}$$

For a 8-cm PCF with the above specified parameters, we arrive at $C \sim 10^6$. This estimate shows that Čerenkov-type phase matching may lead to a substantial improvement in the THG efficiency with respect to the efficiency of THG in confined waveguide modes. A more detailed analysis of Čerenkov phase-matched THG in PCFs should be based on the knowledge of Čerenkov-type modes for a specific PCF structure. This poses the problem of extending the methods of analysis of guided modes in microstructure fibers[37–43] to Čerenkov-type modes.

3. EXPERIMENT

The laser system (Fig. 5) used for our experiments was based on a Cr^{4+}:forsterite laser[44] pumped by an Yb:fiber diode-pumped laser (IPG Photonics, Ltd.). A typical output of the Cr:forsterite laser was ~200 mW of average power at a repetition rate of 27 MHz with an 8-W pump. The central wavelength was 1250 nm, and a typical laser pulse bandwidth was approximately 50 nm.

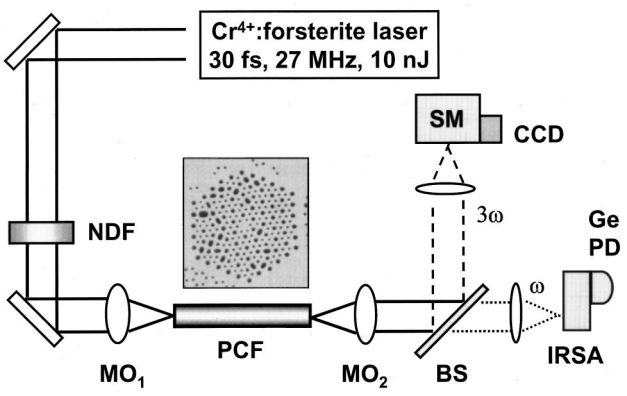

Fig. 5. Diagram of the experimental arrangement for studying the generation of the cross-phase-modulated third harmonic in a PCF. NDF, neutral-density filter; MO_1, MO_2, micro-objectives; BS, beam splitter; IRSA, IR spectrum analyzer; SM, spectrometer; CCD, liquid-nitrogen-cooled CCD camera; Ge PD, Ge photodetector. The inset shows the cross-sectional image of a PCF sample with the pitch of the cladding equal to 1.5 μm and the air-filling fraction equal to 16%.

Unamplified radiation produced by the Cr:forsterite laser was coupled into a PCF (see the inset in Fig. 5). The details of the technology employed to fabricate the PCFs used in our experiments, which was similar to the process developed by Knight *et al.*,[1] are described elsewhere.[11,45,46] Briefly, the fabrication process involved drawing identical glass capillaries stacked into a periodic preform at an elevated temperature, cutting the resulting structure into segments, and repeating the technological cycle again. This procedure allowed the fabrication of PCFs with a cladding pitch ranging from 400 nm to 32 μm.[45,46]

We were able to measure the pulse energies both at the input and at the output of the fiber, which allowed us to estimate the laser energy and power density coupled into the fiber. The third-harmonic intensity was measured with a SPEX 1/4-m spectrometer with an attached liquid-nitrogen-cooled CCD camera, which supported the photon-counting mode. The spectra of transmitted IR radiation were measured by a CVI, Inc., spectrometer with an attached Ge photodiode.

4. RESULTS AND DISCUSSION

Propagation of 30-fs Cr:forsterite laser pulses through a PCF was accompanied by several nonlinear optical effects, which were enhanced by the small size of the fiber core. In experiments with a PCF with a core radius of 1.5 μm, a length of 8 cm, and an air filling fraction of the cladding equal to 16%, we observed spectral broadening of laser pulses due to SPM and the generation of third-harmonic radiation. As shown by Ranka *et al.*,[12] efficient THG becomes possible in microstructure fibers owing to the multimode phase matching of the pump pulse and the third harmonic. In subsection 2.C of this paper we demonstrated that phase matching for THG in PCFs may be improved in the regime in which one of the localized PCF modes of the pump pulse gives rise to a Čerenkov-type emission of the third harmonic. The spectral broadening $\Delta\omega_{\mathrm{SPM}}$ of the pump pulses coming out of the fiber increased with the growth in the laser power coupled into the fiber (Fig. 6). We did not observe any noticeable influence of stimulated Raman scattering on the spectra of pump pulses within the sub-0.5-nJ range of pump energies studied. The SPM-broadened spectra of the pump pulses at the output of the fiber measured in our experiments qualitatively agree with the results of numerical simulations presented in Fig. 1, indicating the adequacy of the qualitative level of our model's approach described in Section 2.

Third-harmonic pulses also appeared spectrally broadened at the output of the fiber. Figure 7 shows typical spectra of the third harmonic produced by 30-fs pulses of Cr:forsterite laser radiation with an energy of 0.3 nJ in a 8-cm PCF sample with a core radius of 1.5 μm and the air-filling fraction of the cladding equal to 16% [Fig. 5(b)]. The spectra of the third harmonic, as can be seen from Fig. 7, display a characteristic asymmetry, which was predicted on the basis of our model approach in Section 2. Moreover, some of the spectral features of the third-harmonic signal can be qualitatively understood in terms of our model, as can be seen from the comparison of the experimental data in Fig. 7 and theoretical predictions of Eqs. (11)–(14).

As can be seen from the comparison of the spectra of pump radiation and of the third harmonic coming out of the fiber (Figs. 6 and 7), the spectra of the third harmonic at the output of the fiber display a much more noticeable asymmetry than the spectra of the pump pulses transmitted through the PCF. This agrees well with our theoretical predictions and indicates that the asymmetry observed in the spectrum of the third harmonic is built in the frequency-conversion process rather than arising primarily at the frequency of the pump pulse and then generating a spectrally distorted third harmonic. On the other hand, the XPM-induced spectral broadening of third-harmonic pulses observed in our experiments starting with very low energies of femtosecond pump pulses (see Fig. 7) offers a convenient way to control the phase of frequency-upconverted ultrashort pulses and even to com-

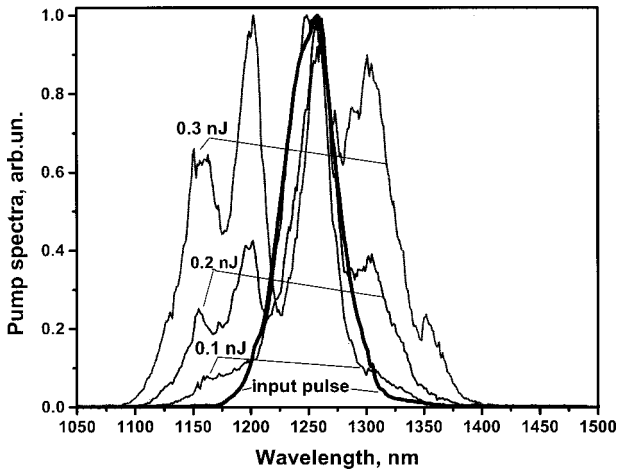

Fig. 6. Normalized spectra of Cr:forsterite laser pulses at the input and at the output of a PCF with a length of 8 cm, the pitch of the cladding equal to 1.5 μm, and an air-filling fraction of 16%. The duration of laser pulses coupled into the fiber is ~30 fs, and their energies are 0.1, 0.2, and 0.3 nJ (as shown near the curves).

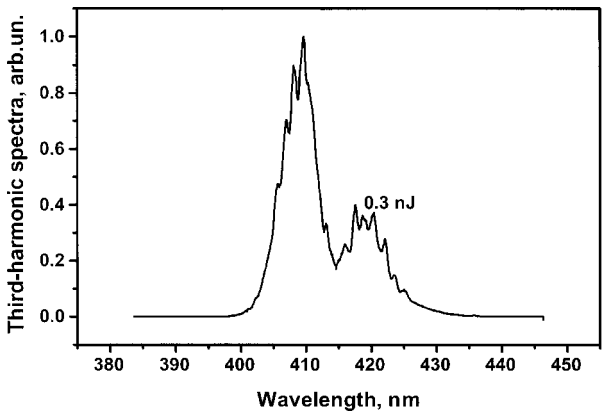

Fig. 7. Normalized spectra of the third harmonic produced by 30-fs Cr:forsterite laser pulses with an energy of 0.3 nJ in a PCF with a length of 8 cm, the pitch of the cladding equal to 1.5 μm, and an air-filling fraction of 16%.

press these pulses through compensation of the XPM-induced phase shift. In the case of gas-filled hollow fibers, a similar method of short-pulse frequency conversion with simultaneous pulse compression was earlier experimentally demonstrated by Durfee *et al.*,[47] who were able to produce 8-fs pulses at the frequency of the third harmonic of Ti:sapphire laser radiation through a two-color four-wave mixing process starting with 35-fs pulses of fundamental radiation. Based on the results of our measurements, we can expect that PCFs may allow phase-controlled frequency conversion, as well as frequency conversion with simultaneous pulse compression, to be implemented with much lower energies of ultrashort laser pulses because of the high degree of localization of the light field in the core of a PCF.

Apart from the possibilities of compressing frequency-upconverted pulses, analysis of XPM in THG is also important for gaining a deeper understanding of nonlinear optical processes contributing to supercontinuum generation. In particular, the measurements performed on the third harmonic in our experiments serve to illustrate how a rather complicated combination of different four-wave mixing processes leads to qualitative spectral transformations of ultrashort pulses propagating in microstructure fibers.

5. CONCLUSION

The results of experiments presented in this paper demonstrate that the high degree of light localization in the core of a microstructure fiber enhances third-order nonlinear optical processes, allowing the third harmonic of nonamplified 30-fs 0.2-nJ Cr:forsterite laser pulses to be generated. Both pump and third-harmonic pulses appeared spectrally broadened at the output of the fiber, indicating a considerable influence of self- and cross-phase modulation (XPM) effects. As the energy of pump pulses coupled into the fiber was increased, the spectra of third-harmonic pulses became broader, at the same time displaying an increasing asymmetry. This asymmetry in third-harmonic spectra can be attributed to variations in the effective wave-vector mismatch Δk_{eff}, which changes from the leading edge of the pump pulse to its trailing edge. Predominant blueshifting of third-harmonic spectra observed in our experiments is then also explained in terms of Δk_{eff} changes, since the effective wave-vector mismatch on the trailing edge of the pump pulse in a nonlinear material with self-focusing is always less than Δk_{eff} on the leading edge of the pump pulse. Our observation of an XPM-chirp-controlled third-harmonic generation process enhanced in a photonic-crystal fiber, in fact, opens the way for using such fibers for frequency conversion of low-energy femtosecond pulses with simultaneous chirp control and subsequent pulse compression.

ACKNOWLEDGMENTS

This study was supported in part by the Volkswagen Foundation (project I/76 869). The work of A. B. Fedotov, A. N. Naumov, and A. M. Zheltikov was also supported in part by President of Russian Federation Grant 00-15-99304, Russian Foundation for Basic Research project 00-02-17567, and Awards RP2-2266 and RP2-2275 of the U.S. Civilian Research and Development Foundation for the Independent States of the former Soviet Union (CRDF). V. V. Yakovlev acknowledges the support of National Science Foundation–ECS Grant 9984225.

A. Naumov can be reached by e-mail at naumov @top.phys.msu.su.

REFERENCES

1. J. C. Knight, T. A. Birks, P. St. J. Russell, and D. M. Atkin, "All-silica single-mode optical fiber with photonic crystal cladding," Opt. Lett. **21**, 1547–1549 (1996).
2. T. A. Birks, J. C. Knight, and P. St. J. Russell, "Endlessly single-mode photonic crystal fiber," Opt. Lett. **22**, 961–963 (1997).
3. J. C. Knight, J. Broeng, T. A. Birks, and P. St. J. Russell, "Photonic bandgap guidance in optical fibers," Science **282**, 1476–1478 (1998).
4. J. C. Knight, T. A. Birks, R. F. Cregan, P. St. J. Russell, and J.-P. De Sandro, "Large mode area photonic crystal fibre," Electron. Lett. **34**, 1347–1348 (1998).
5. J. C. Knight, T. A. Birks, R. F. Cregan, P. St. J. Russell, and J.-P. De Sandro, "Photonic crystals as optical fibres—physics and applications," Opt. Mater. **11**, 143–151 (1999).
6. R. F. Cregan, B. J. Mangan, J. C. Knight, T. A. Birks, P. St. J. Russell, P. J. Roberts, and D. C. Allan, "Single-mode photonic guidance of light in air," Science **285**, 1537–1539 (1999).
7. A. M. Zheltikov, "Holey fibers," Phys. Usp. **170**, 1203–1220 (2000).
8. T. M. Monro, P. J. Bennett, N. G. R. Broderick, and D. J. Richardson, "Holey fibers with random cladding distributions," Opt. Lett. **25**, 206–208 (2000).
9. N. G. R. Broderick, T. M. Monro, P. J. Bennett, and D. J. Richardson, "Nonlinearity in holey optical fibers: measurement and future opportunities," Opt. Lett. **24**, 1395–1397 (1999).
10. J. K. Ranka, R. S. Windeler, and A. J. Stentz, "Visible continuum generation in air–silica microstructure optical fibers with anomalous dispersion at 800 nm," Opt. Lett. **25**, 25–27 (2000).
11. A. B. Fedotov, A. M. Zheltikov, L. A. Mel'nikov, A. P. Tarasevitch, and D. von der Linde, "Spectral broadening of femtosecond laser pulses in fibers with a photonic-crystal cladding," JETP Lett. **71**, 281–285 (2000).

12. J. K. Ranka, R. S. Windeler, and A. J. Stentz, "Optical properties of high-delta air–silica microstructure optical fibers," Opt. Lett. **25**, 796–798 (2000).
13. A. B. Fedotov, A. M. Zheltikov, A. P. Tarasevitch, and D. von der Linde, "Enhanced spectral broadening of short laser pulses in high-numerical-aperture holey fibers," Appl. Phys. B **73**, 181–184 (2001).
14. Th. Udem, J. Reichert, R. Holzwarth, and T. W. Hänsch, "Absolute optical frequency measurement of the cesium D_1 line with a mode-locked laser," Phys. Rev. Lett. **82**, 3568–3571 (1999).
15. S. A. Diddams, D. J. Jones, J. Ye, S. T. Cundiff, J. L. Hall, J. K. Ranka, R. S. Windeler, R. Holzwarth, T. Udem, and T. W. Hänsch, "Direct link between microwave and optical frequencies with a 300 THz femtosecond laser comb," Phys. Rev. Lett. **84**, 5102–5105 (2000).
16. D. J. Jones, S. A. Diddams, J. K. Ranka, A. Stentz, R. S. Windeler, J. L. Hall, and S. T. Cundi, "Carrier-envelope phase control of femtosecond mode-locked lasers and direct optical frequency synthesis," Science **288**, 635–639 (2000).
17. R. Holzwarth, T. Udem, T. W. Hänsch, J. C. Knight, W. J. Wadsworth, and P. St. J. Russell, "Optical frequency synthesizer for precision spectroscopy," Phys. Rev. Lett. **85**, 2264–2267 (2000).
18. T. A. Birks, W. J. Wadsworth, and P. St. J. Russell, "Supercontinuum generation in tapered fibers," Opt. Lett. **25**, 1415–1417 (2000).
19. D. A. Akimov, A. B. Fedotov, A. A. Podshivalov, A. M. Zheltikov, A. A. Ivanov, M. V. Alfimov, S. N. Bagayev, V. S. Pivtsov, T. A. Birks, W. J. Wadsworth, and P. St. J. Russell, "Spectral superbroadening of subnanojoule Cr:forsterite femtosecond laser pulses in a tapered fiber," JETP Lett. **74**, 460–463 (2001).
20. S. N. Bagayev, A. K. Dmitriyev, S. V. Chepurov, A. S. Dychkov, V. M. Klementyev, D. B. Kolker, S. A. Kuznetsov, Yu. A. Matyugin, M. V. Okhapkin, V. S. Pivtsov, M. N. Skvortsov, V. F. Zakharyash, T. A. Birks, W. J. Wadsworth, P. St. J. Russell, and A. M. Zheltikov, "Femtosecond frequency combs stabilized with a He–Ne/CH_4 laser: toward a femtosecond optical clock," Laser Phys. **11**, 1270–1282 (2001).
21. B. E. Bouma, G. J. Tearney, I. P. Bilinsky, B. Golubovic, and J. G. Fujimoto, "Self-phase-modulated Kerr-lens mode-locked Cr:forsterite laser source for optical coherence tomography," Opt. Lett. **21**, 1839–1841 (1996).
22. A. A. Ivanov, M. V. Alfimov, and A. M. Zheltikov, "An all-solid-state sub-40-fs self-starting Cr^{4+}:forsterite laser broadly tunable within therapeutic-window range for high-resolution coherence-domain and nonlinear-optical biomedical applications," Laser Phys. **10**, 796–799 (2000).
23. G. P. Agrawal, *Nonlinear Fiber Optics* (Academic, Boston, 1989).
24. N. I. Koroteev and A. M. Zheltikov, "Chirp control in third-harmonic generation due to cross-phase modulation," Appl. Phys. B **67**, 53–57 (1998).
25. A. M. Zheltikov, N. I. Koroteev, and A. N. Naumov, "Self- and cross-phase modulation accompanying third-harmonic generation in a hollow waveguide," JETP **88**, 857–867 (1999).
26. R. Maleck Rassoul, A. Ivanov, E. Freysz, A. Ducasse, and F. Hache, "Second-harmonic generation under phase-velocity and group-velocity mismatch: influence of cascading self-phase and cross-phase modulation," Opt. Lett. **22**, 268–270 (1997).
27. A. N. Naumov and A. M. Zheltikov, "Asymmetric spectral broadening and temporal evolution of cross-phase-modulated third harmonic pulses," Opt. Express **10**, 122–127 (2002).
28. A. W. Snyder and J. D. Love, *Optical Waveguide Theory* (Chapman & Hall, New York, 1983).
29. I. S. Grigor'ev and E. Z. Meilikhov, eds., *Physical Quantities Handbook* (Energoatomizdat, Moscow, 1991) (in Russian).
30. P. K. Tien, R. Ultich, and R. Martin, "Optical second-harmonic generation in form of coherent Cerenkov radiation from a thin-film waveguide," Appl. Phys. Lett. **17**, 447–450 (1970).
31. N. A. Sanford and W. C. Robinson, "Direct measurement of effective indices of guided modes in $LiNbO_3$ waveguides using the Čerenkov second harmonic," Opt. Lett. **12**, 445–447 (1987).
32. R. Ramponi, R. Osellame, M. Marangoni, and V. Russo, "Near-infrared refractometry of liquids by means of waveguide Čerenkov second-harmonic generation," Appl. Opt. **37**, 1–6 (1998).
33. R. Ramponi, M. Marangoni, R. Osellame, and V. Russo, "Nonconventional characterization of single-mode planar proton-exchanged $LiNbO_3$ waveguides by Cerenkov second harmonic generation," Opt. Commun. **159**, 37–42 (1999).
34. H. Z. Hu, K. Sh. Zhong, D. Q. Tang, and Zh. X. Lu, "Theoretical analysis of Cherenkov frequency-doubling in a periodically poled $LiNbO_3$ waveguide," Opt. Commun. **174**, 105–118 (2000).
35. D. Pezzetta, C. Sibilia, R. Ramponi, R. Osellame, M. Marangoni, M. Bertolotti, J. W. Haus, M. Scalora, M. J. Bloemer, and C. M. Bowden, "Enhanced Čerenkov second-harmonic generation in planar nonlinear waveguide reproducing a one-dimensional photonic bandgap," J. Opt. Soc. Am. B **19**, 2102–2110 (2002).
36. S. A. Akhmanov, V. A. Vysloukh, and A. S. Chirkin, *Optics of Femtosecond Laser Pulses* (American Institute of Physics, New York, 1992).
37. J. Broeng, S. E. Barkou, T. Søndergaard, and A. Bjarklev, "Analysis of air-guiding photonic bandgap fibers," Opt. Lett. **25**, 96–98 (2000).
38. T. M. Monro, D. J. Richardson, N. G. R. Broderick, and P. J. Bennett, "Holey optical fibers: an efficient modal model," J. Lightwave Technol. **17**, 1093–1102 (1999).
39. F. Brechet, J. Marcou, D. Pagnoux, and P. Roy, "Complete analysis of the characteristics of propagation into photonic crystal fibers by the finite element method," Opt. Fiber Technol.: Mater., Devices Syst. **6**, 181–191 (2000).
40. A. Ferrando, E. Silvestre, J. J. Miret, P. Andrés, and M. V. Andrés, "Vector description of higher-order modes in photonic crystal fibers," J. Opt. Soc. Am. B **17**, 1333–1340 (2000).
41. T. M. Monro, D. J. Richardson, N. G. R. Broderick, and P. J. Bennet, "Modeling large air fraction holey optical fibers," J. Lightwave Technol. **18**, 50–56 (2000).
42. T. P. White, R. C. McPhedran, L. C. Botten, G. H. Smith, and C. Martijn de Sterke, "Calculations of air-guided modes in photonic crystal fibers using the multipole method," Opt. Express **9**, 721–732 (2001).
43. A. M. Zheltikov, M. V. Alfimov, A. B. Fedotov, A. A. Ivanov, M. S. Syrchin, A. P. Tarasevitch, and D. von der Linde, "Controlled light localization and nonlinear-optical interactions of ultrashort laser pulses in micro- and nanostructured fibers with a tunable photonic band gap," JETP **93**, 499–509 (2001).
44. V. Shcheslavskiy, V. V. Yakovlev, and A. A. Ivanov, "High-energy self-starting femtosecond Cr^{4+}:Mg_2SiO_4 oscillator operating at a low repetition rate," Opt. Lett. **26**, 1952–1954 (2001).
45. M. V. Alfimov, A. M. Zheltikov, A. A. Ivanov, V. I. Beloglazov, B. A. Kirillov, S. A. Magnitskii, A. V. Tarasishin, A. B. Fedotov, L. A. Mel'nikov, and N. B. Skibina, "Photonic-crystal fibers with a photonic band gap tunable within the range of 930–1030 nm," JETP Lett. **71**, 489–492 (2000).
46. A. B. Fedotov, M. V. Alfimov, A. A. Ivanov, A. V. Tarasishin, V. I. Beloglazov, A. P. Tarasevitch, D. von der Linde, B. A. Kirillov, S. A. Magnitskii, D. Chorvat, D. Chorvat Jr., A. N. Naumov, E. A. Vlasova, D. A. Sidorov-Biryukov, A. A. Podshivalov, O. A. Kolevatova, L. A. Mel'nikov, D. A. Akimov, V. A. Makarov, Yu. S. Skibina, and A. M. Zheltikov, "Holey fibers with 0.4–32-μm-lattice-constant photonic band-gap cladding: fabrication, characterization, and nonlinear-optical measurements," Laser Phys. **11**, 138–145 (2001).
47. C. G. Durfee III, S. Backus, H. C. Kapteyn, and M. M. Murnane, "Intense 8-fs pulse generation in the deep ultraviolet," Opt. Lett. **24**, 697–699 (1999).